Mapping Serotonergic Dynamics using Drug-Modulated Molecular Connectivity

Ionescu TM[1], Amend M[1], Hafiz R[2], Maurer A[1], Biswal BB[2], Wehrl HF[1†], Herfert K[1 †]

1 Werner Siemens Imaging Center, Department of Preclinical Imaging and Radiopharmacy, Eberhard Karls University Tuebingen, Germany

2 Department of Biomedical Engineering, New Jersey Institute of Technology, University Heights, Newark, New Jersey, USA

† contributed equally

Corresponding author:

Prof. Dr. Kristina Herfert (kristina.herfert@med.uni-tuebingen.de)

Address: Roentgenweg 13, 72076 Tuebingen, Germany,

Tel: +49 7071 29 87680

Abstract

Brain imaging plays a critical role in unraveling the complex functional architecture of animal and human brains. However, individual imaging modalities often face limitations confining them to narrow physiological perspectives. Our study introduces "Molecular connectivity" (MC), a novel concept in imaging that provides a detailed view of molecular interactions and their implications for brain functionality. This research bridges the gap between functional magnetic resonance imaging (fMRI) which tracks neurovascular dynamics, and positron emission tomography (PET), revealing molecular changes at the receptor level. The integration of these techniques can enhance our comprehension of brain-wide effects of drugs. In this study, we delve deeper into this integration by extracting molecular connectivity (MC) at the individual subject level using dynamic [^{11}C]DASB PET scans, which map serotonin transporters (SERT). We particularly focus on assessing the ability of this method to track pharmacological alterations introduced by methylenedioxymethamphetamine (MDMA).

Our comprehensive analysis involves a comparison between MC and functional connectivity (FC), utilizing seed-based and independent component analysis (ICA) during resting states. We identified significant, physiologically pertinent independent components with the [^{11}C]DASB data, thereby enhancing the interpretation of FC results. Remarkably, we observed pronounced changes in MC following a single MDMA administration with strong correlations between resting state MC and the spatial-temporal patterns of MDMA´s effect on SERT occupancy.

This research marks a pioneering effort in investigating subject-level MC using PET imaging. Our findings suggests that these advanced imaging techniques can substantially refine our understanding of how drugs influence the overarching functional organization of the brain.

Introduction

The field of neuroscience has witnessed remarkable advancements over the past decade, particularly propelled by the advent of innovative imaging techniques. The simultaneous application of positron emission tomography (PET) and magnetic resonance imaging (MRI) has revolutionized our ability to concurrently assess brain function across various physiological dimensions [1, 2]. This is especially true in the context of drug effect evaluations. The combination of PET with functional MRI (fMRI) has opened a plethora of investigative avenues. Techniques such as resting-state functional connectivity (rs-FC) [3] or pharmacological fMRI (phMRI) [4] are now complemented by the capability of PET to quantify molecular changes, including alterations in receptor and transporter availability [5].

While fMRI provides high spatial and temporal resolution, the interpretation of its readout necessitates caution. The Blood-Oxygen-Level-Dependent (BOLD) signal used in fMRI indirectly captures neuronal changes through neurovascular coupling [6]. This only reveals the hemodynamic consequences of molecular-level drug effects. The integration of simultaneous PET acquisition can bridge this interpretative gap by offering essential molecular insights, particularly regarding transporter or receptor alterations. Typically, PET, used either independently or simultaneously to fMRI, has been mainly used in pharmacological studies for illustrating quantitative shifts in neuroreceptor or transporter availabilities [7]. Several studies have also explored the interregional coherence of PET tracer signals [8-10], an approach akin to fMRI-derived rs-FC. While subject-wise metabolic connectivity using [^{18}F]FDG-PET has been established through the temporal correlation of regional PET signals [1, 8], studies employing transporter or receptor tracers have predominantly focused on interregional binding coherences across subjects using static scans [9, 10]. The concept and feasibility of molecular connectivity (MC) through the temporal correlation of dynamic binding potentials of transporter or receptor tracers have yet to be explored.

In our study, we investigate the feasibility of deriving MC from dynamic [^{11}C]DASB-PET scans acquired simultaneously with fMRI in rats. We divided the rats into two cohorts: a baseline group and a pharmacological application group, exposed to 3,4-methyldeoxymetamphetamine (MDMA). The baseline cohort served to assess the feasibility of the novel methodology, contrasting it with traditional fMRI-derived rs-FC

with a specific focus on temporal stability. We postulated that dynamic [^{11}C]DASB PET temporal fluctuations could be harnessed for connectivity data, in a manner similar to hemodynamic rs-FC, using seed-based and independent component analysis (ICA).

The second cohort, subjected to an MDMA challenge allowed us to evaluate the utility of our novel approach. We aimed to outline the effects of MDMA by integrating the innovative MC concept with established analysis techniques. Our primary objective of this research was to elucidate the potential of PET-derived MC in conjunction with simultaneous PET/fMRI, exploring the avenues this methodology could open for future diagnostic and drug development studies.

Material and Methods

Our study reevaluates two distinct datasets previously published by our group [11, 12], to simultaneously explore FC and MC both at baseline conditions [12] and following MDMA administration [11]. For detailed descriptions on animal handling, experimental setups, and data acquisition procedures, please refer to these earlier publications.

Animals

A total of 41 male Lewis rats were obtained from Charles River Laboratories (Sulzfeld, Germany). Thirty rats underwent baseline [^{11}C]DASB PET/fMRI scans without any pharmacological intervention, while 11 rats underwent [^{11}C]DASB PET/fMRI scans including an acute MDMA challenge. All experiments were conducted in compliance with German federal regulations for experimental animals and received approval from the Regierungspräsidium Tübingen.

Simultaneous PET/fMRI Experiments

The rats were subjected to simultaneous PET/fMRI experiments involving 1.3% isoflurane anesthesia, tail vein catheterization, positioning on a temperature-controlled bed, and monitoring vital signs. The scans were performed using a 7T small-animal ClinScan MRI scanner (Bruker Biospin, Ettlingen, Germany) with a custom-developed PET insert [13]. Both the scanning protocol and the sequence parameters have been outlined in detail in our previous publication [11]. The MDMA

cohort received a pharmacological MDMA challenge of 3.2 mg/kg intravenously 40 minutes after tracer injection.

Data Preprocessing and Analysis

Data preprocessing followed established protocols, including steps such as realignment, mask creation, coregistration, spatial normalization, signal cleaning, and spatial smoothing, as detailed in our previous work [11]. For the MDMA dataset, PET scans were analyzed for early and late effects post-challenge using the general linear model (GLM) available in SPM. For both datasets the baseline was defined 30 to 40 minutes after scan start. For the fMRI data a first level analysis was applied to the individual scans without a high-pass filter (the filter was set to “Inf”). Statistical parametric maps were generated post GLM parameter estimation using contrast vectors. Group-level analysis involved a one-sample t-test on the subject-level statistical parametric maps ($p < 0.05$, one-sided, family wise error / FWE-adjusted).

Static PET scans were generated by summing dynamic frames over defined periods for 10-minute periods after the MDMA challenge (50-60 minutes to investigate early effects, and 70-80 minutes to investigate late MDMA effects). Two-sample t-maps were calculated between the normalized [^{11}C]DASB uptakes of (1) the baseline scan period and the early effect time period and of (2) the early effect time period and the late effect time period ($p < 0.05$, FWE-adjusted).

All group-level t-maps underwent voxel-wise signal quantification to determine the regional contributions of 48 regions selected according to the Schiffer atlas [14]. Average t-scores and standard deviations of all voxels were calculated.

Functional Connectivity Analysis

Functional connectivity was determined using a seed-based analysis approach. The mean time series of the pre-processed BOLD-fMRI signals for each dataset across all regions (refer to *Supplementary Table 1* for the list of regions) were extracted using SPM toolbox Marseille Boîte À Région d’Intérêt (MarsBaR). Pairwise Pearson’s correlation coefficients were calculated between each pair of mean regional time-series for every dataset. The Pearson’s r coefficients were converted into z-values using Fischer’s transformation for group-level analysis. The Fischer’s z-transformed

correlation coefficients were then used to generate mean correlation matrices for both cohorts [15].

Molecular connectivity analysis

The mean [^{11}C]DASB signal from the preprocessed PET datasets was extracted from the designed regions, including the 48 regions used for fMRI data analysis and the cerebellum using MarsBaR. Binding potentials were calculated frame-wise for all dynamic PET scans using the DVR-1 (equation 1) to generate regional BP_{ND} values using the cerebellum as a reference region [16]:

$$BP_{ND} = \frac{V_T - V_{ND}}{V_{ND}} = \frac{V_T}{V_{ND}} - 1 = DVR - 1, \quad (1)$$

where:

- BP_{ND} is the binding potential
- V_T is the total volume of distribution
- V_{ND} is the volume of distribution in a reference tissue
- DVR is the relative volume of distribution

To calculate MC, we discarded the first 20 minutes of every scan, which were dominated by perfusion effects and applied a detrending approach on the remaining 60 minutes in order to obtain temporally stable values (for further details, please refer to Supplementary Methods and Supplementary Figure 1). The BP_{ND} time courses were then used to calculate MC as described above for fMRI: subject-level correlation matrices between all regional time courses were generate and z-transformed correlation coefficients were used to calculate mean correlation matrices.

Independent Component Analysis

Group ICA (GIFT toolbox, MIALAB, University of New Mexico, Albuquerque, NM, USA) was used for ICA of the baseline group. Both the fMRI and PET preprocessed data sets were investigated between 30 and 80 minutes after start of data acquisition. For fMRI, we selected 10 independent components, while we started with two components for PET and increased the number to ten components to thoroughly dissect the varying components within the signal. Components were thresholded at a z-vlaue ≥ 1.96 (p-value ≤ 0.05) [17] and average z-scores and standard deviations

were calculated for each component. These components' physiological significance was further explored by contrasting them with the regional [11C]DASB changes induced by MDMA. Accordingly, the z-scores of the independent components generated in the baseline cohort were correlated with the early and late regional [^{11}C]DASB changes induced by MDMA, measured using t-scores.

Results

Comparability of MC and FC in spatial contexts and over time

We first aimed to evaluate whether MC aligns spatially with FC, possesses similar graph theory properties and provides consistent temporal readouts throughout the scan duration in the baseline group (Figure 1).

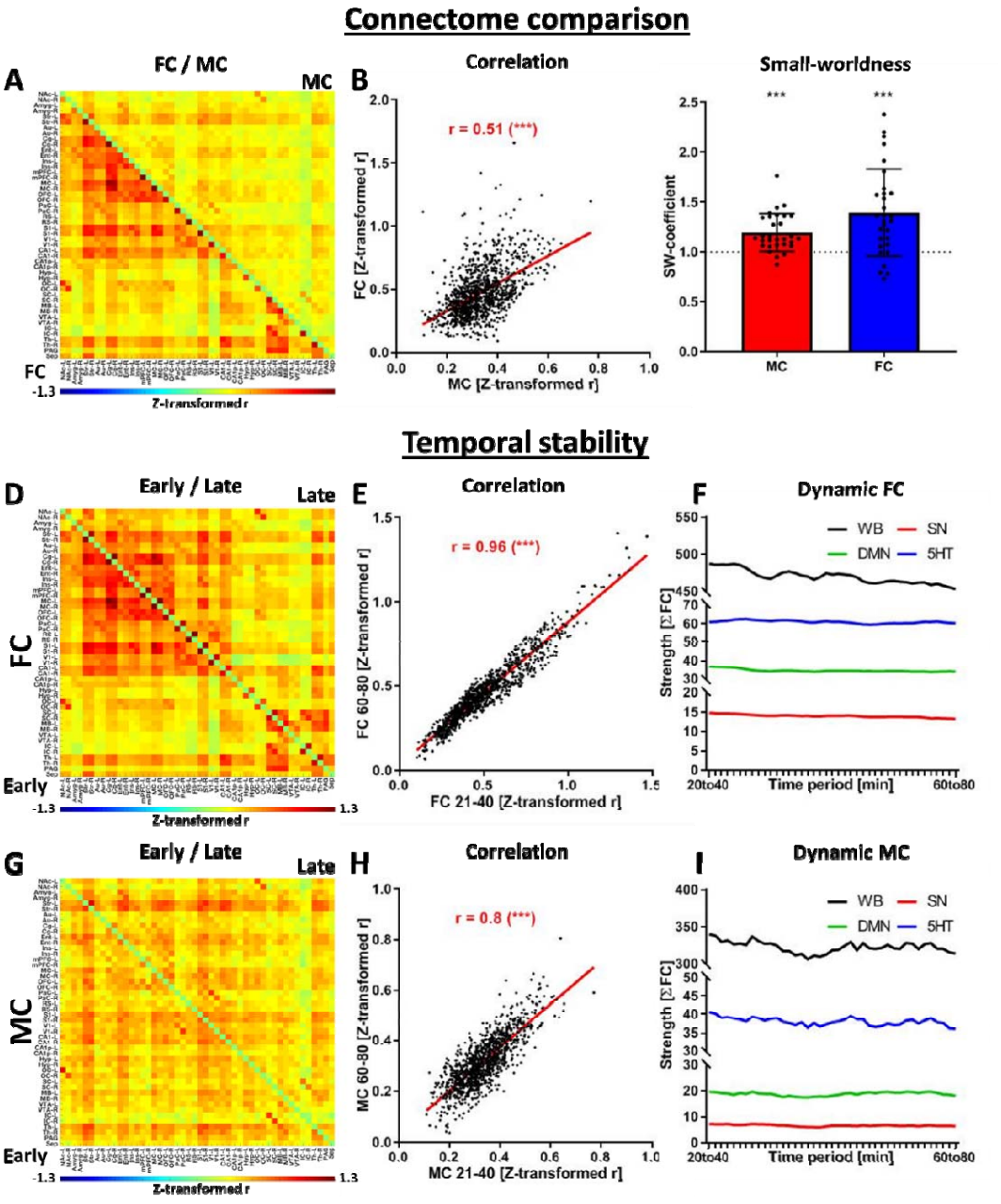

Figure 1: Evaluation of seed-based MC. (A) Correlation matrix indicating whole-brain FC (beneath diagonal) and MC (above diagonal). Correlations not surviving significance testing with multiple comparison corrections were set to zero ($p < 0.05$, FWE correction). **(B)** Scatter plot and correlation between MC and FC edges. **(C)** Small-world coefficients for all subjects and group-level one-sample t-test against the value of 1 (SW > 1 is considered as indicative of small-world properties). Copmarison of **(D)** FC and **(G)** MC early (20-40 minutes after scan start, below diagonal) and late (60-80 minutes after scan start, above diagonal). The similarties of early and late readouts were quantified for both **(E)** FC and **(H)** MC. Temporal stability of both **(F)** FC and **(I)** MC was evaluated using a sliding window approach including 20-minute windows between 20 and 80 minutes after scan start. Abbreviations: FC

= fMRI-derived hemodynamic functional connectivity, MC = [^{11}C]DASB PET-derived molecular connectivity.

We found moderate, but significant correlation between the edge-level MC and FC ($r = 0.51$, $p < 0.001$, Figure 1A and B). Furthermore, both connectomes revealed small-world properties at group-level, with coefficients higher than 1 (Figure 1C). At subject level, three molecular and four functional connectomes fell below the threshold of 1 for the small-world coefficient. A significant consistency was observed betweeen early and late scan-derived connectomes (Figure 1D for FC, G for MC), with FC having a slight edge (Figure 1E, $r = 0.96$) over MC (Figure 1H, $r = 0.8$). While both, FC and MC maintained steady correlation intensities, there was a negligable decline over the scan duration (Figure 1F and 1I).

Deciphering spatial characteristics of FC and MC using ICA

After establishing the feasibility of obtaining temporally stable readouts using the ROI-to-ROI approach, we employed a data-driven approach, using ICA, to compare spatial characteristics of FC and MC (Figure 2).

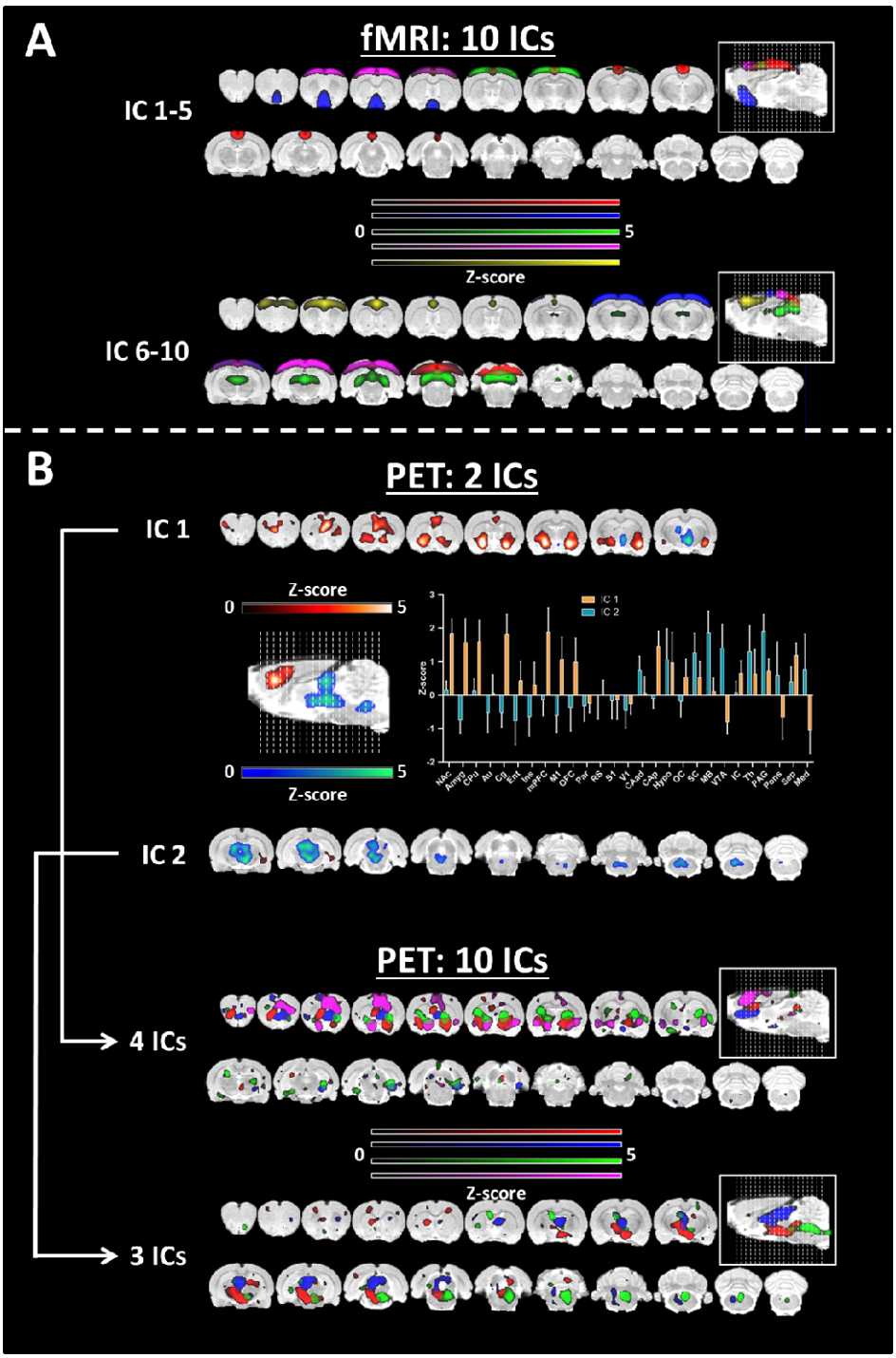

Figure 2: Group independent component analysis for FC and MC. (A) ICA performed over 10 components for fMRI. **(B)** ICA performed over 2 components for [^{11}C]DASB PET and regional quantification of the two derived components. The ICA was repeated over 10 components. Four and three components showed good overlap with the two components defined above. All components were thresholded at $z > 1.96$ ($p \leq 0.05$). Abbreviations: FC = fMRI-derived hemodynamic functional connectivity, MC = [^{11}C]DASB PET-derived molecular connectivity.

We extracted ten group ICs from the fMRI data (Figure 2A), revealing known canonical resting-state networks, such as the posterior default-mode-like network (IC1-5, red), sensorimotor networks (IC1-5, green and purple), the anterior default-mode-like network (IC6-10, yellow) or the visual network (IC6-10, red). With unpredictability for the number of ICs suitable for MC IC extraction, we started with two components (Figure 2B). IC1 (orange) comprised both subcortical and cortical anterior brain regions, including the nucleus accumbens, amygdala, cingulate cortex, caudate putamen, orbitofrontal cortex and medial prefrontal cortex, while IC2 (blue) primarily received contributions from deeper posterior areas, such as the midbrain, thalamus, hypothalamus, periaquaeductal gray and medulla. Interestingly, when we extracted 10 independent components, to mimic the number of components used for the FC data, we found that the initial anterior component split in four different ICs and the initial posterior IC in three different ICs. A relatively clear spatial segregation can be seen for the newly-formed ICs, for instance the three posterior components being extracted from specific regions (green mainly from medulla, red from hypothalamus and part of the midbrain, blue from midbrain and thalamus).

MDMA-induced changes of ICA-derived molecular connectivity

Next, we aimed to explore the relationship between molecular changes in SERT availability and the molecular connectome derived from ICA, induced by an acute MDMA administration (Figure 3).

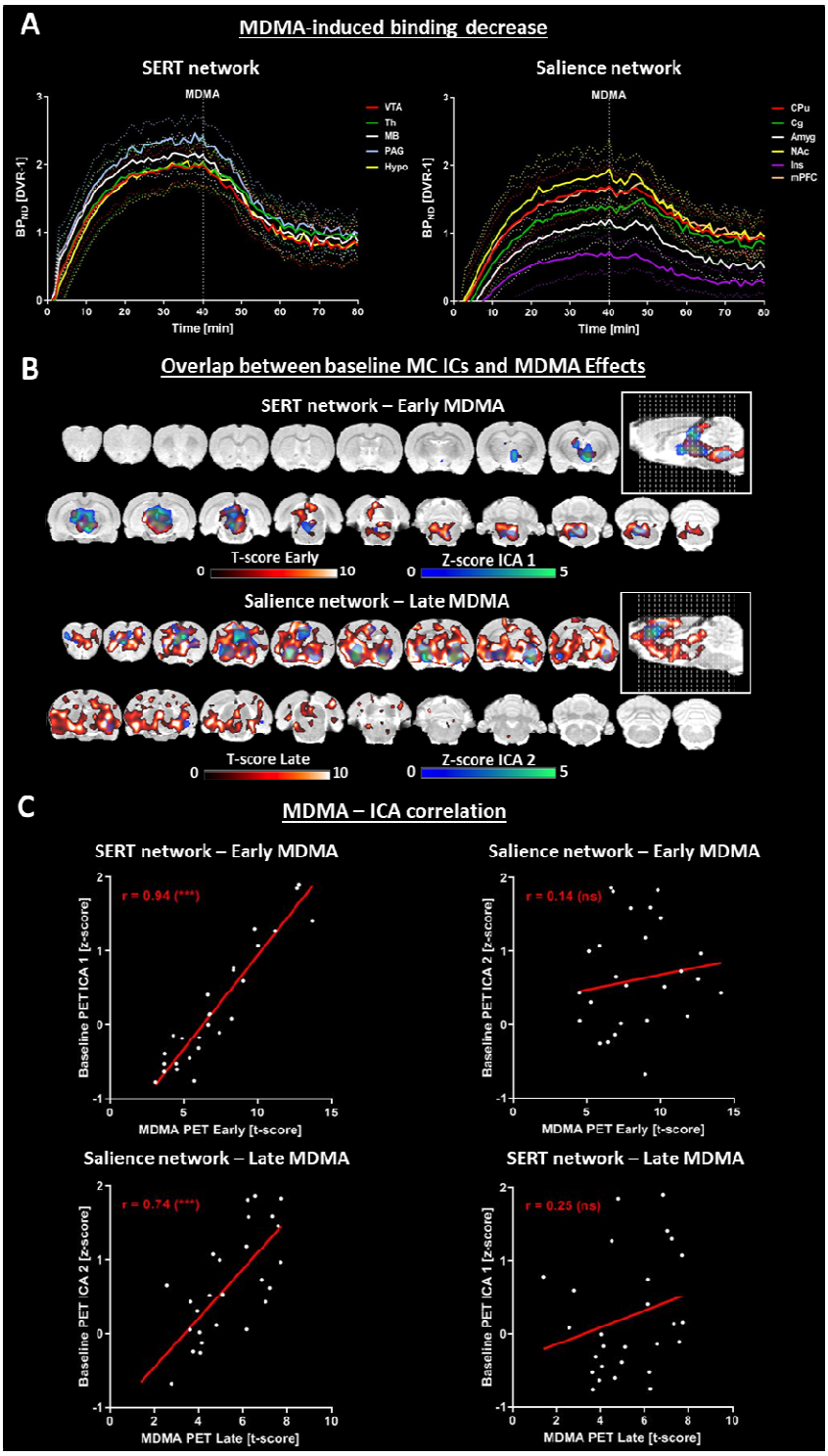

Figure 3: Comparison of MDMA-induced [^{11}C]DASB alterations. (A) Left panel: Dynamic binding potentials of regions comprising SERT network, defined by IC 1 in validation cohort. Right panel: Dynamic binding potentials of regions comprising salience network, defined by IC 1 in validation cohort. **(B)** Overlap between independent components extracted from the validation cohort (IC 1 = SERT network; IC 2 = salience network) and the early and late effects of MDMA respectively. **(C)** Pair-

wise correlations between regional z-scores of the ICs extracted from validation cohort and regional t-scores of early and late MDMA effects. (*** indicates $p < 0.001$, ns = non-significant). Abbreviations: SERT = serotonin transporter, ICA = independent component analysis; for abbreviations of regions please refer to *Supplementary Information*).

Two IC extracted from the MC showed good overlap with regions associated with the salience network (IC1) and with those having high SERT densities (IC2). Therefore, we defined the regions contributing strongly to IC1 as salience network (CPu, Cg, NAc, Amyg, Ins, mPFC) and those with strong signals in IC2 as SERT network (VTA, Th, MB, PAG, Hypo). Interestingly, MDMA induced immediate strong decreases in all SERT network regions, salience areas exhibited a delay by approximately 10 minutes (Figure 3A). Voxel-level analysis showed clear spatial overlaps between early MDMA responsive regions and those from the posterior IC, with delayed regions mirroring the anterior IC reminiscent of the salience network (Figure 3B). To quantify the striking spatial similarity between the baseline independent components and the spatiotemporal characteristics of [^{11}C]DASB changes after MDMA exposure, we show highly significant correlations between the z-scores of the posterior and anterior ICs and the t-scores of late and early MDMA effects on [^{11}C]DASB alterations, respectively ($p < 0.0001$, Figure 3C).

Finally, we investigated relationships between SERT availability changes and MC reductions following the acute MDMA challenge (Figure 4).

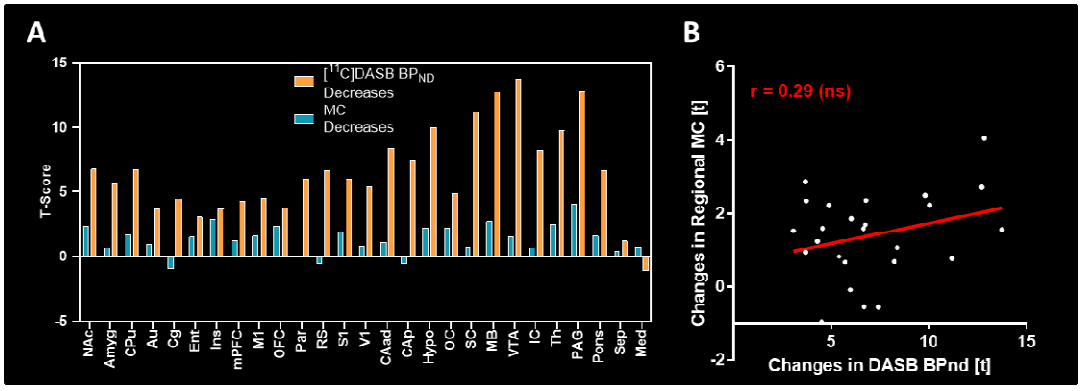

Figure 4: Comparison of MC and BP_{ND} changes. A Reduction in BP_{ND} following MDMA (orange) and MC strength (blue) was compared. **B** T-scores derived from each approach show only low correlations.

We found that the decreases in MC and in [^{11}C]DASB BP_{ND} following MDMA application (Figure 4A) showed only low correlation (r = 0.29, Figure 4B). While

decreases in SERT availability exhibited a strong anterior-posterior gradient, being most pronounced in areas with high SERT availability, such as the MB, VTA, Pons or PAG, MC encompassed regions across the brain to similar extents. Specifically, while the significance of [^{11}C]DASB reductions in the Ins was very low across investigated regions, the Ins showed highest effects among regions for MC, while strong SERT occupancy effects in the IC and SC did not translate in very prominent reductions in the respective global MC of the two regions.

MDMA-induced changes of seed based molecular connectivity

Next, we performed a seed-based analysis and aimed to compare changes in FC and MC after an MDMA pharmacological challenge on the salience network and on regions with high SERT binding (Figure 5).

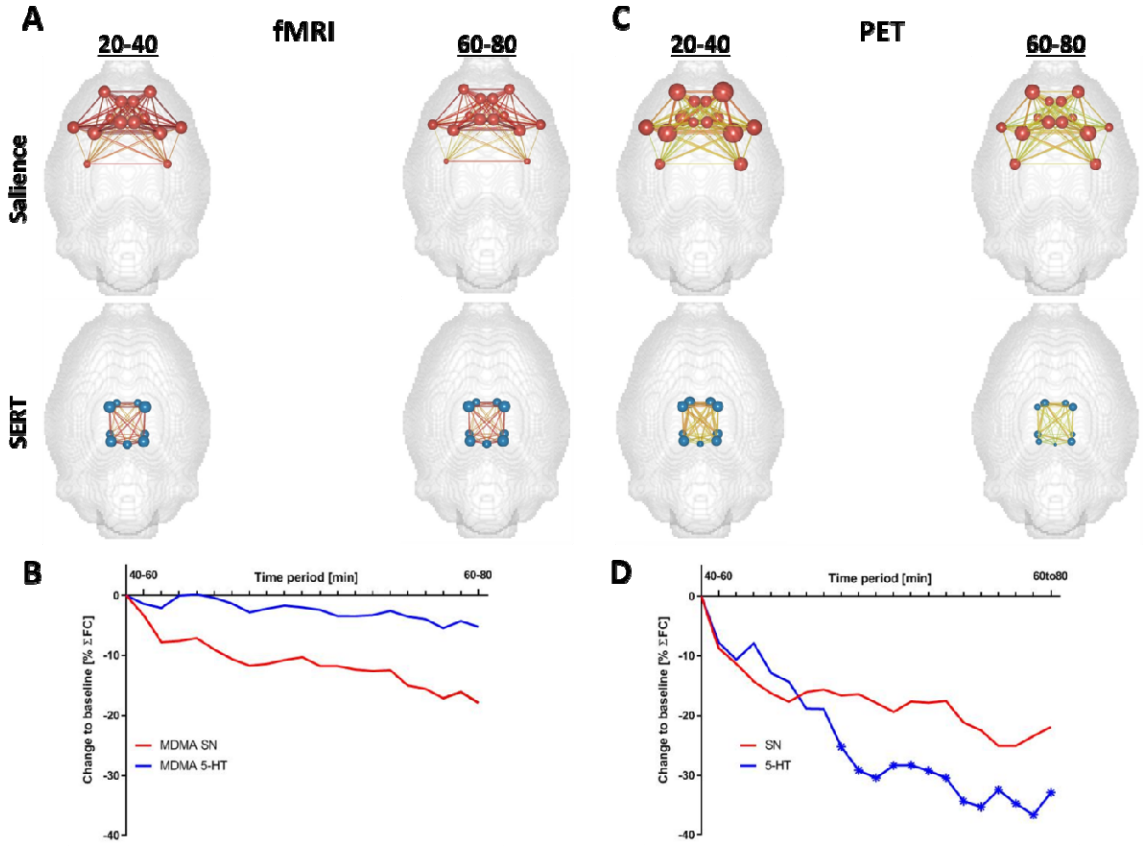

Figure 5: MDMA effects on seed-based FC and MC of the salience and SERT networks. (A) FC and **(C)** MC brain networks depicting edge and node strengths of the salience network and SERT network at baseline (20-40 min after scan start) and after MDMA (60-80 min after scan start). **(B)** FC and **(D)** MC time-resolved salience and SERT network strengths computed using sliding windows. Asterisks indicate significant ($p < 0.05$, FDR-corrected) changes to baseline (time-point zero,

corresponding to 20-40 minutes after scan start). Abbreviations: SN = salience network, SERT = SERT network.

We observed a small decrease in the SN for FC (16% at the end of the scan) and almost constant FC of the SERT network (<5% decrease) following MDMA, as shown in Figure 5A at edge and node level and Figure 5C at network level ($p>0.05$). For MC, we observed profound reductions in the SERT network (Figure 5C and D), emphasizing an acute and spatially specific effect of MDMA on MC.

Discussion

The mammalian brain operates on diverse physiological, spatial and temporal scales. FC via BOLD-fMRI offers insights into coherent functional brain networks, but its complexity and indirect link to neural activity highlight the need for more direct methodologies. In this context, the concept of MC using [^{11}C]DASB PET, as introduced in our study, provides a more direct and complementary perspective on brain organization and its response to external stimuli, such as MDMA.

Physiological basis

Our findings suggest that [^{11}C]DASB binding reflect the interplay of serotonin levels and SERT dynamics [18]. Supporting the competition model, evidence indicates that endogenous serotonin competes with tracers for binding sites, affecting tracer binding [19]. However, contrasting results in various studies highlight the complexity of this interaction [20] [21] [22]. The internalization model suggests serotonin levels influence SERT internalization, impacting [^{11}C]DASB binding [18, 23, 24]. While supporting evidence exists, further exploration is needed to fully understand these dynamics, especially during resting states [25]. Some models on this aspect have proposed a regulatory function of the raphé nuclei in maintaining serotonin fluctuations over several temporal scales at rest [26]. Remarkably, fast microdialysis has resolved multiple spontaneous surges of up to 1500-fold of the basal serotonin occurring during 30-minute intervals [27]. Additionally, the same study has indicated that SERT expression is essential for the spontaneous surges, reduced SERT drastically decreasing serotonin spiking. Thus, it is feasible that the correlated temporal fluctuations captured by dynamic [^{11}C]DASB at least partly reflect the role of the serotonergic system in brain resting activity.

Implications for whole-brain serotonergic system

Our graph-theory analysis revealed comparable whole-brain organization between hemodynamic and serotonergic connectomes, although we only found moderate correlation between the edges of the two measurements. Notably, the correlations in [^{11}C]DASB bindings differed from BOLD-fMRI-derived correlations. For BOLD-fMRI, ICA revealed classic RSNs, widely reported for both rats [28] and humans [29], including the default-mode network, the sensory network and the motor network. In contrast, the ICA analysis of PET data revealed two distinct anatomical modules. The first component included primarily the brainstem, parts of the midbrain and the thalamus. The second component comprised regions of the limbic system, such as the striatum, amygdala, insular, cingulate and prefrontal cortices, reflecting the diverse projections of the raphe nuclei. The distinct anatomical modules identified in the ICA analysis of PET data reflect the diverse projections of raphe nuclei, suggesting a complex serotonergic system response to drugs. MDMA's interaction with SERT, as elucidated by [^{11}C]DASB, shows region-specific temporal effects, with immediate decreases in binding in the brainstem and posterior subcortical regions, and delayed effects in limbic pathways. This suggests that the serotonergic system's response to drugs can be predicted, to an extent, by the observed independent components.

Relevance to prior research

Our findings align with those by Salvan et al [31] on the integration of molecular maps into fMRI data demonstrating how individual serotonergic receptors contribute to network-level activity. Despite our differing methodologies, the receptor activity patterns they found, may also correspond to the different independent components we found from the [^{11}C]DASB PET data. The dual regression approach reported by Salvan et al. has first been reported in the context of pharmacology to delineate the receptor-specific effects of MDMA in humans [32]. The authors found that MDMA specifically decreased FC in the 5HT1A maps in areas which could be ascribed to the human salience network, such as the insula and a collection of medial cortical regions. While not reaching significance, we observed in reduced salience FC and MC in our data.

Previous studies evaluating the effects of MDMA on FC indicated relatively sparse effects on FC, as confirmed by the readout of this study [33, 34]. Recently, a novel approach [32] has revealed decreased connectivity induced by MDMA in areas associated with SERT and 5-HT_{1A} availability. The increased activity indicated in limbic and cortical structures when controlling for vascular effects is accompanied with decreased salience connectivity, indicating that, while neurons become more active through the drug, they do so in an incoherent manner, which would be in line with the hyperactive, yet abnormal behavior reported for MDMA abuse. Importantly, the potent vascular effects which play a role in modulating the amplitude of the BOLD-fMRI signal may also influence FC readouts, although the extent of such effects are difficult to estimate.[11]

Over the past decade, PET studies using [^{11}C]DASB have focused on the associations of serotonin transporter (SERT) availabilities across different brain regions, revealing altered interregional SERT connections in patient cohorts, post-treatment changes, and predictive capacity for treatment response [9, 10, 35] [36] [37]. Our study builds upon this foundation, uncovering significant within-subject temporal associations in [^{11}C]DASB binding, and demonstrates more pronounced alterations in MC compared FC changes induced by drugs, thus highlighting the enhanced utility of our method.

Study limitations and future directions

While our study advances the understanding of MC, the use of anesthetized animal is a limitation, potentially affecting PET and fMRI readouts and their interaction with MDMA. Future studies should involve awake animals to validate our method. Additionally, our multimodal imaging approach, though powerful, cannot fully decipher the mechanisms of interregional coherences in PET timecourses. Future studies employing sensitive methods to measure neurotransmitter release, could provide deeper insights into the molecular processes underpinning our observations.

Nonetheless, we provide several strong arguments to consider such analyses as presented here in future studies. First, we show that at rest the data are reliable, temporally stable and exhibiting similar graph theory metrics to traditionally calculated functional connectomes. Second, in spite of comparable network-level organizational properties, already at rest MC is only moderately correlated to FC, indicating the

complementary nature of both readouts. Third, resting-state MC ICs correlate well with SERT occupancy changes induced by the MDMA challenge. Finally, we show that the changes MDMA elicits on MC are complementary to standardly-calculated [^{11}C]DASB BP_{ND} alterations. Our data indicate that, while changes in BP_{ND} are more pronounced in regions with higher baseline SERT availabilities, MC reveals a more globally distributed measure of tracking serotonergic changes, since also regions, such as the insula, with relatively low SERT expressions, were strongly affected.

Conclusion

This study significantly contributes to integrating molecular data into connectomic frameworks, demonstrating that subject-level MC is reliable and complementary to FC in both resting and pharmacologically challenged states. Our research lays a strong foundation for future investigations into the value and generalizability of PET-derived MC, particularly for understanding drug-induced brain-wide molecular network changes.

Bibliography

1. Wehrl, H.F., et al., *Simultaneous PET-MRI reveals brain function in activated and resting state on metabolic, hemodynamic and multiple temporal scales.* Nat Med, 2013. **19**(9): p. 1184-9.
2. Judenhofer, M.S., et al., *Simultaneous PET-MRI: a new approach for functional and morphological imaging.* Nat Med, 2008. **14**(4): p. 459-65.
3. Biswal, B., et al., *Functional connectivity in the motor cortex of resting human brain using echo-planar MRI.* Magn Reson Med, 1995. **34**(4): p. 537-41.
4. Jonckers, E., et al., *The power of using functional fMRI on small rodents to study brain pharmacology and disease.* Frontiers in Pharmacology, 2015. **6**(231).
5. Sander, C.Y., et al., *Neurovascular coupling to D2/D3 dopamine receptor occupancy using simultaneous PET/functional MRI.* Proceedings of the National Academy of Sciences of the United States of America, 2013. **110**(27): p. 11169-11174.
6. Buxton, R.B., *Dynamic models of BOLD contrast.* NeuroImage, 2012. **62**(2): p. 953-961.
7. Silberbauer, L.R., et al., *Serotonin Transporter Binding in the Human Brain After Pharmacological Challenge Measured Using PET and PET/MR.* Frontiers in Molecular Neuroscience, 2019. **12**(172).
8. Amend, M., et al., *Functional resting-state brain connectivity is accompanied by dynamic correlations of application-dependent [(18)F]FDG PET-tracer fluctuations.* Neuroimage, 2019. **196**: p. 161-172.

9. Lanzenberger, R., et al., *Prediction of SSRI treatment response in major depression based on serotonin transporter interplay between median raphe nucleus and projection areas.* Neuroimage, 2012. **63**(2): p. 874-81.
10. Vanicek, T., et al., *Altered interregional molecular associations of the serotonin transporter in attention deficit/hyperactivity disorder assessed with PET.* Human Brain Mapping, 2017. **38**(2): p. 792-802.
11. Ionescu, T.M., et al., *Neurovascular Uncoupling: Multimodal Imaging Delineates the Acute Effects of 3,4-Methylenedioxymethamphetamine.* J Nucl Med, 2023. **64**(3): p. 466-471.
12. Ionescu, T.M., et al., *Striatal and prefrontal D2R and SERT distributions contrastingly correlate with default-mode connectivity.* Neuroimage, 2021. **243**: p. 118501.
13. Disselhorst, J.A., et al., *NEMA NU 4-2008 performance evaluation and MR compatibility tests of an APD-based small animal PET-insert for simultaneous PET/MR imaging.* Phys Med Biol, 2022. **67**(4).
14. Schiffer, W.K., et al., *Serial microPET measures of the metabolic reaction to a microdialysis probe implant.* J Neurosci Methods, 2006. **155**(2): p. 272-84.
15. Xia, M., J. Wang, and Y. He, *BrainNet Viewer: A Network Visualization Tool for Human Brain Connectomics.* PLOS ONE, 2013. **8**(7): p. e68910.
16. Walker, M., et al., *In Vivo Evaluation of 11C-DASB for Quantitative SERT Imaging in Rats and Mice.* J Nucl Med, 2016. **57**(1): p. 115-21.
17. Di, X., B.B. Biswal, and I. Alzheimer's Disease Neuroimaging, *Metabolic brain covariant networks as revealed by FDG-PET with reference to resting-state fMRI networks.* Brain Connect, 2012. **2**(5): p. 275-83.
18. Paterson, L.M., et al., *Measuring Endogenous 5-HT Release by Emission Tomography: Promises and Pitfalls.* Journal of Cerebral Blood Flow & Metabolism, 2010. **30**(10): p. 1682-1706.
19. Yamamoto, S., et al., *Effects of increased endogenous serotonin on the in vivo binding of [11C]DASB to serotonin transporters in conscious monkey brain.* Synapse, 2007. **61**(9): p. 724-731.
20. Lundquist, P., et al., *Effect on [11C]DASB binding after tranylcypromine-induced increase in serotonin concentration: Positron emission tomography studies in monkeys and rats.* Synapse, 2007. **61**(6): p. 440-449.
21. Talbot, P.S., et al., *Effects of reduced endogenous 5-HT on the in vivo binding of the serotonin transporter radioligand 11C-DASB in healthy humans.* Synapse, 2005. **55**(3): p. 164-175.
22. Lefevre, A., et al., *Oxytocin and Serotonin Brain Mechanisms in the Nonhuman Primate.* The Journal of Neuroscience, 2017. **37**(28): p. 6741-6750.
23. Ramamoorthy, S. and R.D. Blakely, *Phosphorylation and Sequestration of Serotonin Transporters Differentially Modulated by Psychostimulants.* Science, 1999. **285**(5428): p. 763-766.
24. Blakely, R.D., et al., *Regulated phosphorylation and trafficking of antidepressant-sensitive serotonin transporter proteins.* Biological Psychiatry, 1998. **44**(3): p. 169-178.
25. Raichle, M.E. and D.A. Gusnard, *Appraising the brain's energy budget.* Proceedings of the National Academy of Sciences, 2002. **99**(16): p. 10237-10239.
26. Salomon, R.M. and R.L. Cowan, *Oscillatory serotonin function in depression.* Synapse, 2013. **67**(11): p. 801-820.

27. Yang, H., et al., *Physiologically relevant changes in serotonin resolved by fast microdialysis.* ACS chemical neuroscience, 2013. **4**(5): p. 790-798.
28. Becerra, L., et al., *Robust reproducible resting state networks in the awake rodent brain.* PLoS One, 2011. **6**(10): p. e25701.
29. Fox, M.D., et al., *The human brain is intrinsically organized into dynamic, anticorrelated functional networks.* Proc Natl Acad Sci U S A, 2005. **102**(27): p. 9673-8.
30. Shih, J.-H., et al., *Evaluation of brain SERT occupancy by resveratrol against MDMA-induced neurobiological and behavioral changes in rats: A 4-[18F]-ADAM/small-animal PET study.* European Neuropsychopharmacology, 2016. **26**(1): p. 92-104.
31. Salvan, P., et al., *Serotonin regulation of behavior via large-scale neuromodulation of serotonin receptor networks.* Nat Neurosci, 2023. **26**(1): p. 53-63.
32. Dipasquale, O., et al., *Receptor-Enriched Analysis of functional connectivity by targets (REACT): A novel, multimodal analytical approach informed by PET to study the pharmacodynamic response of the brain under MDMA.* NeuroImage, 2019. **195**: p. 252-260.
33. Carhart-Harris, R.L., et al., *The Effects of Acutely Administered 3,4-Methylenedioxymethamphetamine on Spontaneous Brain Function in Healthy Volunteers Measured with Arterial Spin Labeling and Blood Oxygen Level–Dependent Resting State Functional Connectivity.* Biological Psychiatry, 2015. **78**(8): p. 554-562.
34. Roseman, L., et al., *The effects of psilocybin and MDMA on between-network resting state functional connectivity in healthy volunteers.* Frontiers in human neuroscience, 2014. **8**: p. 204-204.
35. James, G.M., et al., *Effects of Selective Serotonin Reuptake Inhibitors on Interregional Relation of Serotonin Transporter Availability in Major Depression.* Frontiers in Human Neuroscience, 2017. **11**(48).
36. Hahn, A., et al., *Attenuated serotonin transporter association between dorsal raphe and ventral striatum in major depression.* Human brain mapping, 2014. **35**(8): p. 3857-3866.
37. Hahn, A., et al., *Escitalopram enhances the association of serotonin-1A autoreceptors to heteroreceptors in anxiety disorders.* J Neurosci, 2010. **30**(43): p. 14482-9.